

# The relation between stellar magnetic field geometry and chromospheric activity cycles I: The highly variable field of $\epsilon$ Eridani at activity minimum

S. V. Jeffers,<sup>1</sup> S. Boro Saikia<sup>1</sup> J. R. Barnes,<sup>2</sup> P. Petit,<sup>3,4</sup> S. C. Marsden,<sup>5</sup>

M. M. Jardine,<sup>6</sup> A. A. Vidotto,<sup>7</sup> and the BCool collaboration <sup>★</sup>

<sup>1</sup>*Institut für Astrophysik, Georg-August-Universität, Friedrich-Hund-Platz 1, 37077 Göttingen, Germany*

<sup>2</sup>*School of Physical Sciences, The Open University, Walton Hall, Milton Keynes MK7 6AA, UK*

<sup>3</sup>*Université de Toulouse, UPS-OMP, Institut de Recherche en Astrophysique et Planétologie, Toulouse, France*

<sup>4</sup>*Institut de Recherche en Astrophysique et Planétologie, 14 Avenue Edouard Belin, F-31400 Toulouse, France*

<sup>5</sup>*Computational Engineering and Science Research Centre, University of Southern Queensland, Toowoomba, 4350, Australia*

<sup>6</sup>*SUPA, School of Physics and Astronomy, University of St Andrews, North Haugh, St Andrews, Fife KY 16 9SS, UK*

<sup>7</sup>*School of Physics, Trinity College Dublin, the University of Dublin, Dublin-2, Ireland*

Accepted XXX. Received YYY; in original form ZZZ

## ABSTRACT

The young and magnetically active K dwarf  $\epsilon$  Eridani exhibits a chromospheric activity cycle of about 3 years. Previous reconstructions of its large-scale magnetic field show strong variations at yearly epochs. To understand how  $\epsilon$  Eridani’s large-scale magnetic field geometry evolves over its activity cycle we focus on high cadence observations spanning 5 months at its activity minimum. Over this timespan we reconstruct 3 maps of  $\epsilon$  Eridani’s large-scale magnetic field using the tomographic technique of Zeeman Doppler Imaging. The results show that at the minimum of its cycle,  $\epsilon$  Eridani’s large-scale field is more complex than the simple dipolar structure of the Sun and 61 Cyg A at minimum. Additionally we observe a surprisingly rapid regeneration of a strong axisymmetric toroidal field as  $\epsilon$  Eridani emerges from its S-index activity minimum. Our results show that all stars do not exhibit the same field geometry as the Sun and this will be an important constraint for the dynamo models of active solar-type stars.

**Key words:** stars – individual ( $\epsilon$  Eridani), stars – activity

## 1 INTRODUCTION

The evolution of the Sun’s large-scale magnetic field ranges from dipolar at activity minimum to complex at activity maximum DeRosa et al. (2012). A solar-like magnetic cycle has also been observed in the K-dwarf 61 Cyg A, where its large-scale field is a simple dipole at activity minimum. In this paper we investigate the evolution of the large-scale magnetic field of  $\epsilon$  Eridani which is well established to be a magnetically active star Valenti et al. (1995) and Metcalfe et al. (2013). Previously in Jeffers et al. (2014), we reconstructed the large-scale magnetic field geometry of  $\epsilon$  Eridani to understand how the photospheric large-scale magnetic field geometry of  $\epsilon$  Eridani varies over its S-index cycle. These observations comprise 6 epochs spanning nearly 7 years or approximately 2 S-index cycles. We showed that each map has evolved

dramatically from one epoch to the next, and that we clearly reconstruct the weakest magnetic field structures at its Ca II H&K (or S-index) minimum. The motivation for this present work is to investigate the evolution of  $\epsilon$  Eridani’s large-scale magnetic field with a higher cadence of observations over its S-index minimum to understand how its field evolution differs from the Sun and 61 Cyg A. To achieve this, we obtained spectropolarimetric observations every night, weather permitting, over a period of five months.

## 2 OBSERVATIONS AND DATA ANALYSIS

We observed  $\epsilon$  Eridani over a time span of 5 months from September 2014 to January 2015 using the high-resolution spectropolarimeter NARVAL located at the Telescope Bernard Lyot, France (Aurière 2003). The total data set comprises 40 spectra which were obtained every night with acceptable observational conditions and are summarised in Table 2. The data were reduced and processed following an identical procedure already explained in Section 3 of Jeffers et al. (2014).

<sup>★</sup> Based on observations made through OPTICON with Telescope Bernard Lyot (TBL, Pic du Midi, France) of the Observatoire Midi-Pyrénées, which is operated by the Institut National des Sciences de l’Univers of the Centre National de la Recherche Scientifique (CNRS) of France.

**Table 1.** Stellar Parameters

Parameter	Value	Reference
Magnitude	V=3.7	
Spectral Type	K2V	Valenti & Fischer (2005)
Distance	3.2 pc	van Leeuwen (2007)
Effective Temperature	5146±31 K	Valenti & Fischer (2005)
Mass ( $M_{\odot}$ )	0.856 <sup>+0.006</sup> <sub>-0.008</sub>	Valenti & Fischer (2005)
Radius ( $R_{\odot}$ )	0.74±0.01	Baines & Armstrong (2012)
$v \sin i$ (km s <sup>-1</sup> )	2.2 <sup>+0.04</sup> <sub>-0.04</sub>	Brewer et al. (2016)
$P_{\text{rot}}$ (day)	11.68	Donahue et al. (1996)
Inclination	46±2°	Jeffers et al. (2014)
Age	440 Myr	Barnes (2007)

All *Stokes I* and *Stokes V* reduced spectra were processed using LSD (Least-Squares Deconvolution Donati et al. 1997). By extracting the information contained in each spectral line, LSD enables the recovery of weak signatures in the line profile despite the presence of noise. The result is one high signal-to-noise spectral profile for each observation. To achieve this, a line list for a star with:  $T_{\text{eff}}$  5000K,  $\log g$  4.5, a depth threshold of 0.1 and  $\log MH$  0.1 and containing 12220 lines was downloaded from the VALD database. This model atmosphere was used to generate a spectral weighting mask. This mask was applied to each observation (comprising a subset of 4 exposures with different polarimeter angles) with a step size of 1.8 km s<sup>-1</sup>, matching NARVAL's detector pixel resolution. The resulting *Stokes V* profiles, which when convolved with the model line profile best matches the observed spectrum of the target star is shown in the outer panels of Figure 1. To parameterise the amount of emission in the Ca II H&K values we use an S-index calculated as described in Jeffers et al. (2014), where the S-index values calculated using NARVAL spectra are calibrated to the values from the Mount Wilson S-index survey by Marsden et al. (2014).

### 3 LARGE-SCALE MAGNETIC FIELD GEOMETRY

The large-scale magnetic field geometry is reconstructed using the tomographic technique of Zeeman-Doppler imaging which incorporates the maximum entropy algorithm described by Skilling & Bryan (1984). This method uses the stellar parameters shown in Table 1 to model local *Stokes V* profiles sampled over the stellar surface from which a disk integrated synthetic *Stokes V* profile is computed. This is then used to iteratively fit the model *Stokes V* profiles to the observed *Stokes V* profiles. The tomographic images of the large-scale magnetic field topology of  $\epsilon$  Eridani are reconstructed by assuming that the field geometry is projected onto a spherical harmonics frame (Donati et al. 2006), where the magnetic energy is decomposed into poloidal and toroidal components. A spherical harmonics expansion with  $\ell_{\text{max}}$  10 was used as there was no improvement to the fits using larger values. A reduced  $\chi^2$  of 1.05 was obtained for all of the maps when differential rotation was included in the image reconstruction process.

#### 3.1 Magnetic maps

The reconstructed large scale magnetic field is shown in the central panels of Figure 1. The observed and the modelled *Stokes V* LSD profiles are shown to the sides of the magnetic maps. Over the 5 month timespan of the observations there is a significant

**Table 2.** Journal of Observations. Phase = 0 is defined as Julian date = 2454101.5 and is used for all epochs, with subsequent epochs taking phase = 0 as an integer number of rotational periods from this value. The exposure time of all observations is 400s.

Date	Julian Date (+2454000)	UT	Phase	LSD S/N	S-index
Map 1 (2014.71)					
01sep14	2902.67	04:05:45	-1.1737	39478	0.402
02sep14	2903.68	04:24:48	-1.0870	36435	0.396
03sep14	2904.67	04:00:01	-1.0029	37224	0.395
05sep14	2906.65	03:38:55	-0.8329	42847	0.394
11sep14	2912.65	03:33:12	-0.3195	35636	0.404
12sep14	2913.62	02:53:49	-0.2362	38801	0.399
13sep14	2914.66	03:47:37	-0.1474	39293	0.396
23sep14	2924.64	03:16:40	0.7069	38855	0.405
24sep14	2925.6	02:19:16	0.7891	36714	0.396
25sep14	2926.62	02:52:49	0.8767	35734	0.403
27sep14	2928.61	02:36:02	1.0469	35976	0.391
Map 2 (2014.84)					
16oct14	2947.65	03:36:25	-1.3227	30832	0.396
17oct14	2948.49	23:49:35	-1.2506	34626	0.395
18oct14	2949.63	03:09:04	-1.1531	36745	0.392
19oct14	2950.58	01:59:09	-1.0717	28518	0.393
24oct14	2955.48	23:37:39	-0.6520	29839	0.405
25oct14	2956.56	01:23:13	-0.5601	36520	0.403
26oct14	2957.44	22:40:33	-0.4842	24285	0.410
28oct14	2959.59	02:07:25	-0.3006	33182	0.402
29oct14	2960.53	00:47:06	-0.2198	36670	0.401
30oct14	2961.49	23:39:16	-0.1382	33682	0.397
31oct14	2962.51	00:13:05	-0.0506	36824	0.401
01nov14	2963.51	00:10:47	0.0349	42832	0.403
12nov14	2974.53	00:45:23	-1.0213	20765	0.388
15nov14	2977.48	23:38:01	-0.7684	31998	0.309
20nov14	2982.45	22:45:26	-0.3435	21015	0.387
Map 3 (2014.98)					
02dec14	2994.39	21:21:14	-2.3211	28400	0.387
02dec14	2994.40	21:32:10	-2.3204	29646	0.387
03dec14	2995.40	21:30:49	-2.2349	38856	0.390
03dec14	2995.40	21:41:47	-2.2342	38417	0.390
19dec14	3011.39	21:17:49	-0.8658	42049	0.385
19dec14	3011.39	21:28:46	-0.8652	39688	0.384
21dec14	3013.40	21:38:44	-0.6933	39051	0.392
21dec14	3013.41	21:49:41	-0.6927	37356	0.392
06jan15	3029.36	20:35:57	0.6728	39935	0.390
06jan15	3029.37	20:46:56	0.6735	39952	0.389
10jan15	3033.36	20:36:39	1.0153	41780	0.384
10jan15	3033.37	20:47:36	1.0160	41215	0.385
17jan15	3040.33	19:56:13	1.6122	31182	0.380
17jan15	3040.34	20:07:11	1.6129	32611	0.379

evolution of the large-scale magnetic field topology of  $\epsilon$  Eridani. The total observations were divided up into three epochs to avoid the presence of large gaps without observations, resulting from poor weather conditions. The division of the observations into the maps was tested for different combinations of observations (e.g. five maps versus three maps) and the result was comparable to the maps presented in Figure 1, though a slightly lower  $\chi^2$  was obtained for the data set divided into three maps. We extensively tested the phase coverage of the maps by assigning random phases to the epochs of observation which resulted in a very similar configuration of magnetic features. We determine the differential ro-

tation of the magnetic features, as described in Jeffers et al. (2014), using the first two epochs which was calculated to be  $\Omega_{eq} = 0.593 \text{ rad d}^{-1}$ ,  $\delta\Omega = 0.151 \text{ rad d}^{-1}$ , which is equivalent to  $P_{eq} = 10.58\text{d}$  and the  $P_{pole} = 14.21\text{d}$ . This is in agreement with our previous measurements of differential rotation for  $\epsilon$  Eridani using magnetic features Jeffers et al. (2014). Other differential rotation measurements for  $\epsilon$  Eridani have been measured using photometric data taken with the MOST satellite where values of 11.35 days, 11.55 days are measured for two different spots (Croll et al. 2006), or  $P_{min} = 11.04$  days and  $P_{max} = 12.18$  days by Donahue et al. (1996). While all of these values broadly agree, the differences can be explained by each method measuring different features, e.g. plage regions, photometry and magnetic features which do not necessarily probe the same depth in the stellar atmosphere or stellar latitudes. Since there are a range of vsini values in the literature we also reconstructed the ZDI maps for an inclination of  $30^\circ$  corresponding to the lowest vsini value of  $1.7 \pm 0.3 \text{ km s}^{-1}$  (Saar & Osten 1997). To fit the Stokes V profiles required a higher  $\chi^2$  value to fit the images (1.12 compared to 0.99 for map1). In the reconstructed maps, high latitude features are slightly less extended in latitude and longitude, though not more than 5-10 degrees, for the radial component. The meridional and azimuthal components show a slight increase in the strength of the features of the order of 10%. We conclude that the use of a lower inclination does not have any significant impact on the reconstructed features in the ZDI maps.

Even though the phase coverage of the last map is not optimal we note that there is significant evolution of the Stokes V profiles between the same rotation phase (phase 0.67), which can be taken into account when differential rotation is included in the reconstruction of the maps. Additionally, for map 3, we note that the Stokes V profiles have the largest amplitudes and that a simple magnetic field topology is expected.

### 3.1.1 Radial component

The radial component of  $\epsilon$  Eridani's large-scale magnetic field is dominated by a persistent and large polar magnetic spot of positive polarity which varies in strength and shape. The strength of the region is highest in 2014.98 (map 3), and weakest in 2014.84 (map 2) while the global shape ranges in latitude from  $30^\circ$  (2014.84) to  $60^\circ$  (2014.98). The strongest evolution of the magnetic field is from epoch 2014.84 (map 2) to epoch 2014.98 (map 3) where the polar spot has increased in strength and evolved into a large spot that is no longer centered at the pole and extends to much lower latitudes. This evolution of magnetic features is also evident in the corresponding Stokes V profiles. Additionally, there are weaker magnetic spots with negative polarity that are likely to be evolving from one epoch to the next. The strength of the negative regions is highest at epochs 2014.98 (map 3) and 2014.71 (map 1) and very weak in 2014.84 (map 2).

### 3.1.2 Azimuthal component

The azimuthal component of  $\epsilon$  Eridani's large-scale field appears only very weakly with small hints of magnetic spots at epochs 2014.71 (map 1) and 2014.98 (map 3). The azimuthal field is strongest at epoch 2014.84 (map 2) where a large magnetic spot of negative polarity extending from phases 0 to 0.3.

### 3.1.3 Meridional component

The determination of the meridional field is often difficult due to the cross talk between the meridional and the radial field. As discussed by Donati & Brown (1997), the cross talk between the radial and meridional fields primarily effects magnetic features at low latitudes, which implies that the higher latitude features are reliably reconstructed. This is evident in the magnetic maps, where the reconstructed negative polarity magnetic features at latitudes  $0^\circ$  to  $50^\circ$  in the meridional field maps are mirrored in the radial field maps (for all maps). The presence of high latitude meridional field in Map 2 at phase 0.5, is considered to be reliable. An additional important consideration is if the cross-talk is from radial to meridional or vice versa. As discussed by Donati & Brown (1997), for stars with low inclinations ( $i < 30^\circ$ ), the cross talk is from radial to meridional while for higher inclinations ( $i > 50^\circ$ ), the cross talk will be from meridional to radial. Since the adopted inclination of  $\epsilon$  Eridani is  $46^\circ$ , it lies between these two possibilities and it is not possible to conclude in which direction the cross talk occurs.

## 3.2 Magnetic energy

Over a period of approximately 5 months,  $\epsilon$  Eridani's large-scale field evolves (as shown in Fig. 2 and Table 3) with decreasing S-index. The most dramatic changes are seen in the rapid emergence of an axisymmetric toroidal field. This is indicated by the colour of the points in Figure 2 changing from red in 2014.71 (map 1) to green in 2014.98 (map 3). The field is notably more complex than a simple dipole at all epochs with significant amounts of the magnetic energy being contained in higher order modes. The poloidal component is approximately 50% dipolar (with values ranging from 43% in 2014.71 to 56% in 2014.84), with additional contributions from the quadrupolar (with an average of 20%) the octupolar component (which are typically of the order of 20%) and higher order modes  $l > 3$ . The axisymmetry of the large-scale field is quite constant with an average value of 35%.

## 4 DISCUSSION

The large-scale magnetic field geometry of  $\epsilon$  Eridani has been shown to be highly variable over its 2.95 year chromospheric activity cycle when observed at yearly epochs (Jeffers et al. 2014). To investigate the evolution on shorter timescales of the magnetic field geometry of  $\epsilon$  Eridani, we secured observations over a period of five successive months, from September 2014 to January 2015, spanning  $\epsilon$  Eridani's chromospheric activity minimum. The large-scale magnetic field is shown to vary on a timescale of months with the first magnetic map reconstructed for epoch 2014.68 (map 1) showing significant evolution compared to the final map reconstructed for epoch 2014.98 (map 3). The large-scale magnetic field geometry is predominantly poloidal (ranging from 74% to 84%) throughout  $\epsilon$  Eridani's activity minimum and in contrast to the rest of its activity cycle where it is also seen to have a strong toroidal components (Jeffers et al. 2014). The poloidal field is not a simple dipole but is quite complex with significant fractions in higher order modes such as quadrupolar and octupolar modes.

The reconstructed complex poloidal field is in contrast to the Sun where its large-scale field is a simple dipole at activity minimum and becomes complex at activity maximum (?). On the Sun, the dipolar and quadrupolar modes vary in anti-phase, such that

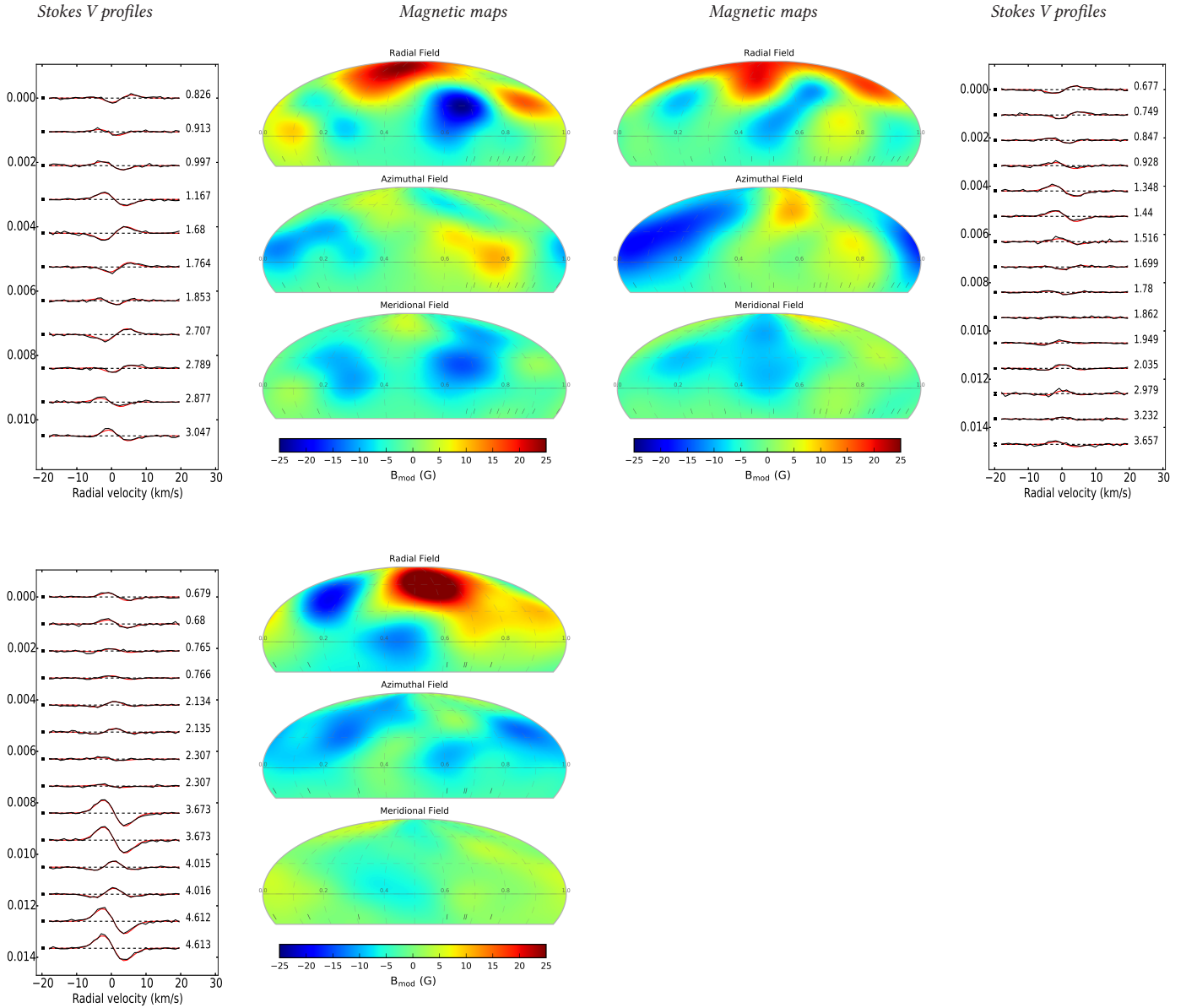


**Figure 1.** Magnetic field maps of  $\epsilon$  Eridani reconstructed for 2014.71, 2014.84 and 2014.98, shown with the *Stokes V* fits to the sides (ordered left to right and top to bottom). For each image the magnetic field projection is shown in terms of radial (upper), azimuthal (middle), and meridional (lower) field components, where red indicates positive polarity and blue negative polarity. The magnetic field strength is in Gauss where for each map the scale is identical ( $B_{\max} = 25$  G). The tick marks at the top of each radial field map indicate the observational phases used to reconstruct the large-scale magnetic field geometry. The *Stokes V* profiles are plotted separated by a constant value for clarity.

after cycle minimum, the quadrupolar mode grows as the number of spots increases, reaching a maximum at cycle maximum (?). However, on  $\epsilon$  Eridani, we observe a slight decrease in the quadrupolar mode at this phase, accompanied by a slight growth in the dipole mode. The changes are small, and a longer term study is needed to confirm if this is indeed the pattern that characterises the cycle. The most significant change in  $\epsilon$  Eridani's large-scale magnetic field is in the toroidal component of the axisymmetric field which evolves from 5% to 72% precisely at the emergence of  $\epsilon$  Eridani from its activity minimum and shows a strong axisymmetry, just like the Sun's poloidal field. Currently, there is limited information on the long-term evolution of the Sun's toroidal field as only a few years of vector data are available (Gosain et al. 2013;

Vidotto 2016). Within this small time window, however, the solar toroidal field was much weaker than on  $\epsilon$  Eridani. A longer term comparison of the variation of the toroidal field over the stellar magnetic cycle may shed some light on the nature of the magnetic cycle.

Another star that has been monitored as part of the BCoOL survey and that has stellar parameters very similar to  $\epsilon$  Eridani is 61 Cyg A (Boro Saikia et al. 2016), which also exhibits a solar-like magnetic cycle. At activity minimum, the large-scale field of 61 Cyg A is also a simple dipole like the solar case, showing that it is not a limitation of ZDI that we do not see similar behaviour for  $\epsilon$  Eridani. The poloidal field of  $\epsilon$  Eridani is more complex at activity minimum compared to 61 Cyg A and to the Sun. The S-



**Table 3.** The fraction of the large-scale magnetic energy reconstructed in the toroidal and poloidal field components; the fraction of the poloidal field in the dipolar ( $\ell=1$ ), quadrupolar ( $\ell=2$ ) and octupolar ( $\ell=3$ ) components; and the fraction of the energy stored in the axisymmetric component ( $m=0$ ) (e.g. the fraction of the poloidal field that is axisymmetric and the fraction of the toroidal field that is axisymmetric.)

Epoch	Bmean (G)	Bmax (G)	Toroidal (% tot)	Poloidal (% tot)	Dipolar (% pol)	Quadrupolar (% pol)	Octupolar (% pol)	$\ell > 3$ (% pol)	Axisymmetric (% tot)	Poloidal (% axi)	Toroidal (% axi)
2014.71	$8 \pm 1$	28	16	84	43	25	19	13	35	41	5
2014.84	$8 \pm 1$	20	23	77	56	14	14	16	32	28	43
2014.98	$10 \pm 1$	33	26	74	50	19	22	9	40	29	72

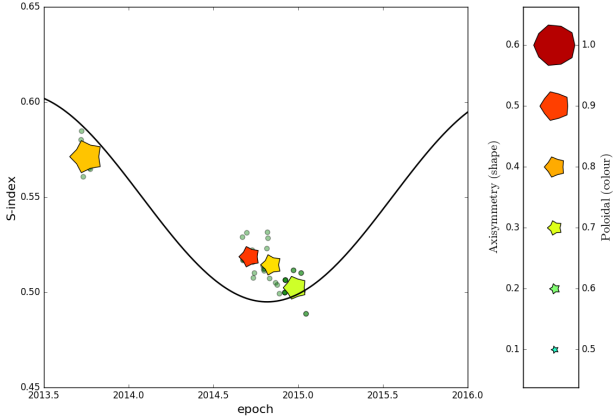


**Figure 2.** The evolution of  $\epsilon$  Eridani’s large-scale field during S-index minimum. The symbol shape indicates the axisymmetry of the field (non axisymmetric by pointed star shape and axisymmetric by decagon), the colour of the symbol indicates the proportion of poloidal (red) and toroidal (blue) components of the field and the symbol size indicates the magnetic field strength. Additionally, S-index points before and after the activity minimum are included (from Jeffers et al. 2014) and unpublished data. The black line indicates the sinusoidal period of 2.95 days and epoch of S-index minimum using the values of Metcalfe et al. (2013).

index cycle of 61 Cyg A is  $7.2 \pm 1.3$  years long (Boro Saikia et al. 2016) and its stellar parameters are more similar to  $\epsilon$  Eridani than the Sun’s. The mass of 61 Cyg A is  $0.66 M_{\odot}$  (Kervella et al. 2008) which is slightly smaller than  $\epsilon$  Eridani’s mass of  $0.7 M_{\odot}$  and given their low  $v \sin i$  values, the ZDI technique has a similar resolving power for both stars. The evolutionary state of the two stars is similar with  $\epsilon$  Eridani having an age that is approximately 7% of its main-sequence lifetime compared to 14% for 61 CygA (calculated using the stellar evolution models of Pols et al. 1998). The main difference is the rotation periods of the two stars, with 61 Cyg A having a rotation period that is approximately three times as long, 35.4 days compared to  $\epsilon$  Eridani’s 11.68 days.

The strength of the mean magnetic field remains constant despite the changing field geometry. In contrast to this, the maximum strength varies from 20 G to 33 G. Since this is the strength in the large-scale component, there is likely to be additional contributions from small-scale component that remains undetected with techniques such as ZDI. Evidence for additional small scale field is shown by magnetic field measurements using *Stokes I* (unpolarised) line broadening which measures the strength of both the large-scale and the small-scale field. These values are typically of the order of 127 G (Valenti et al. 1995) or 165 G (Rüedi et al. 1997). As found by previous authors, the large-scale field is of the order of 10% of the total field. The maximum and mean magnetic field strengths measured in 2014.9 (map3) are comparable to previ-

ous values reconstructed at activity minimum (Jeffers et al. 2014, epoch 2011.81). Additionally at epoch 2011.81, the large-scale field geometry has a large magnetic spot with positive polarity which is very similar to the map reconstructed in 2014.9 (map 3). The two maps have the same fraction of poloidal field (74% for both maps), which has a much more complex structure in 2014.9 compared to 2011.81. The main difference between the two maps is the fraction of axisymmetric field which for epoch 2014.9 comprises 40% and 2011.81 comprises 63%. However, over the three epochs of this analysis there are dramatic changes in the geometry of the axisymmetric field which evolves from 41% to 29% for the poloidal component and 5% to 72% for the toroidal component.

## 5 CONCLUSIONS

The high cadence observations of  $\epsilon$  Eridani’s large-scale magnetic field geometry shows that the large-scale magnetic field geometry evolves on a timescale of months with a dramatic increase in the toroidal component of the axisymmetric field at the emergence from its activity minimum. The large-scale field also shows a predominantly poloidal component that is surprisingly complex when compared to the Sun at activity minimum. Our results show that the magnetic field of solar-type stars can be quite different from the Sun even when they exhibit clear chromospheric activity cycles.

## ACKNOWLEDGMENTS

We would like to thank M.Mengel, B. Carter, C. Folsom and V. See for valuable contributions in discussing the results of this paper, and G. Anglada Escude and A. Reiners for their contributions to the observing proposal. JRB was supported by the UK Science and Technology Facilities Council (STFC) under the grant ST/L000776/1. The research leading to these results has received funding from the European Community’s Seventh Framework Programme (FP7/2013-2016) under grant agreement number 312430 (OPTICON).

## REFERENCES

- Aurière M., 2003, in Arnaud J., Meunier N., eds, EAS Publications Series Vol. 9, EAS Publications Series. p. 105
- Baines E. K., Armstrong J. T., 2012, *ApJ*, **744**, 138
- Barnes S. A., 2007, *A&A*, **669**, 1167
- Boro Saikia S., et al., 2016, *A&A*, **594**, A29
- Brewer J. M., Fischer D. A., Valenti J. A., Piskunov N., 2016, *ApJ*, **225**, 32
- Croll B., et al., 2006, *AJ*, **648**, 607
- DeRosa M. L., Brun A. S., Hoeksema J. T., 2012, *ApJ*, **757**, 96
- Donahue R. A., Saar S. H., Baliunas S. L., 1996, *ApJ*, **466**, 384
- Donati J.-F., Brown S. F., 1997, *A&A*, **326**, 1135

- Donati J.-F., Semel M., Carter B. D., Rees D. E., Collier Cameron A., 1997, *MNRAS*, 291, 658
- Donati J.-F., et al., 2006, *MNRAS*, 370, 629
- Gosain S., Pevtsov A. A., Rudenko G. V., Anfinogentov S. A., 2013, *ApJ*, 772, 52
- Jeffers S. V., Barnes J. R., Jones H. R. A., Reiners A., Pinfield D. J., Marsden S. C., 2014, *MNRAS*, 438, 2717
- Kervella P., et al., 2008, *A&A*, 488, 667
- Marsden S. C., et al., 2014, *MNRAS*, 444, 3517
- Metcalf T. S., et al., 2013, *ApJ*, 763, L26
- Pols O. R., Schröder K.-P., Hurley J. R., Tout C. A., Eggleton P. P., 1998, *MNRAS*, 298, 525
- Rüedi I., Solanki S. K., Mathys G., Saar S. H., 1997, *A&A*, 318, 429
- Saar S. H., Osten R. A., 1997, *MNRAS*, 284, 803
- Skilling J., Bryan R. K., 1984, *MNRAS*, 211, 111
- Valenti J. A., Fischer D. A., 2005, *ApJ*, 159, 141
- Valenti J. A., Marcy G. W., Basri G., 1995, *ApJ*, 439, 939
- Vidotto A. A., 2016, *MNRAS*, 459, 1533
- van Leeuwen F., 2007, *A&A*, 474, 653

This paper has been typeset from a  $\text{\TeX}/\text{\LaTeX}$  file prepared by the author.